Fluidized-bed reactor for methanol synthesis. A theoretical investigation

ARTICLE *in* INDUSTRIAL & ENGINEERING CHEMISTRY RESEARCH · OCTOBER 1991

Impact Factor: 2.59 · DOI: 10.1021/ie00058a009

Solubility studies with Ethocel ether derivatives have given Hansen partial solubility parameters in the range of nonpolar (δ_d) = 16.6–17.3, polar (δ_p) = 6.6–8.3, and hydrogen bond (δ_h) of 8.5–10.0 $MPa^{1/2}$.

Literature Cited

Barton, A. F. M. *Handbook of Solubility Parameters and Other Cohesion Parameters*; CRC Press: Boca Raton, FL, 1983.
Barton, A. F. M. *Handbook of Polymer-Liquid Interaction Parameters and Solubility Parameters*; CRC Press: Boca Raton, FL, 1990.
Dante, M. F.; Bittar, A. D.; Caillault, J. J. *Mod. Paint Coat.* **1989**, *Sept*, 46–51.
Ekman, K. H.; Linfberg, J. *Svom. Kem. B* **1966**, *39*, 89–96.
Entwistle, C. A.; Rowe, R. C. *J. Pharm. Pharmacol.* **1979**, *31*, 269–272.
Hansen, C. M. *J. Paint Technol.* **1967**, *39* (505), 104–117.
Hansen, C. M. *Ind. Eng. Chem. Prod. Res. Dev.* **1969**, *8* (1), 2–11.
Hansen, C. M.; Andersen, B. H. *Am. Ind. Hyg. Assoc. J.* **1988**, *49* (6), 301–308.
Hercules Inc. *Klucel Hydroxypropyl cellulose*; Technical Information Bulletin VC-477C; 1984; p 5.
Kent, D. J.; Rowe, R. C. *J. Pharm. Pharmacol.* **1978**, *30*, 808–810.
Klein, E.; Smith, J. K. *Ind. Eng. Chem. Prod. Res. Dev.* **1972**, *11* (2), 207–210.
Klein, E.; et al. *Water Res.* **1975**, *9*, 807.
Lindberg, J. *Svom. Kem. B* **1967**, *40*, 225–228.
Lindberg, J. *Fin. Kemistsamf. Medd.* **1968**, *70*, 130–141.
Mulder, M. H. V.; Kruitz, F.; Smolders, C. A. *J. Membr. Sci.* **1982**, *11*, 349–363.
Phuoc, N. H.; et al. *J. Pharm. Sci.* **1986**, *75* (1), 68–72.
Phuoc, N. H.; et al. *Int. J. Pharm.* **1987**, *34*, 217–223.
Rowe, R. C. *J. Pharm. Pharmacol.* **1986**, *38*, 214–215.
Rowe, R. C. *Int. J. Pharm.* **1988**, *41*, 219–222.
Sakellariou, P.; Rowe, R. C.; White, E. F. T. *Int. J. Pharm.* **1986a**, *31*, 175–177.
Sakellariou, P.; Rowe, R. C.; White, E. F. T. *Int. J. Pharm.* **1986b**, *34*, 93–103.
Schuerch, C. *J. Am. Chem. Soc.* **1952**, *74*, 5061–5067.
Shareef, K. M. A.; et al. *J. Coating Technol.* **1986**, *58* (733), 35–44.
Teas, J. P. *J. Paint Technol.* **1968**, *40* (516), 19.
Turbak, A. F.; Hammer, R. B.; Davies, R. E.; Hergert, H. L. *Chemtech* **1980**, *Jan*, 51–57.

Received for review March 25, 1991
Revised manuscript received June 3, 1991
Accepted June 26, 1991

PROCESS ENGINEERING AND DESIGN

Fluidized-Bed Reactor for Methanol Synthesis. A Theoretical Investigation

K. M. Wagialla and S. S. E. H. Elnashaie*

Chemical Engineering Department, College of Engineering, King Saud University, P.O. Box 800, Riyadh 11421, Saudi Arabia

Fluidized-bed technology is compared against fixed-bed technology for the production of methanol from synthesis gas. The two-phase theory of fluidization is used to model and simulate the fluidized bed. The model takes into consideration the change in the number of moles accompanying the reaction. An industrial modern quench type fixed-bed methanol synthesis converter is used as a basis for comparison. The fluidized bed resulted in a 30% improvement in the methanol production rate. The efficiency of the fluidized bed is due to the elimination of diffusional limitations, giving rise to an effectiveness factor very close to unity, and also because of the shift of equilibrium to more favorable conditions, which is due to the removal of products of reaction by diffusion from the dense phase to the bubble phase. Simulation of a fluidized-bed case with minimized effect of back-mixing shows a 51.1% improvement in production rate over the industrial fixed-bed reactor.

1. Introduction

Improvements in production efficiency of important chemicals by only a few percents can sometimes result in significant profit increases, energy conservation, and environmental protection, especially for a chemical such as methanol with a worldwide annual production rate of 3.6 $\times 10^6$ tons (Schack et al., 1989).

Higher conversions in conventional methanol converters have been thwarted by equilibrium thermodynamic limitations due to the reversibility of the reaction(s) involved (Graaf et al., 1990). Also diffusional limitations due to relatively large catalyst particles cannot be eliminated in fixed-bed configurations by usage of smaller particles because of the attendant excessive pressure drop in the reactor.

Research efforts for improvement of production efficiency have been largely directed toward the search for more active catalysts and improvement of fixed-bed-reactor design configurations to achieve better energy utilization, smaller reactor size, and higher per-pass conversion. Of late there has been a growing interest in the exploration of the technical and economic viability of reactor types other than the conventional fixed-bed design (Öztürk et al., 1988; Kuczynski et al., 1987a,b).

With regard to catalysis, a very significant change occurred in the late sixties when ICI (Imperial Chemical Industries) introduced its low-pressure methanol synthesis

* To whom correspondence should be addressed.

0888-5885/91/2630-2298$02.50/0

catalysts (Öztürk et al., 1988). These type of catalysts are copper based ($Cu/ZnO/Al_2O_3$ or $Cu/ZnO/Cr_2O_3$). Typical reaction conditions are T = 200–270 °C, P = 50–100 atm, and feed gas composition: CO, 8–10%; CO_2, 5–6%; and the balance being hydrogen (Villa et al., 1985).

Judging from recent research activities, it seems that more efficient methanol production processes will result from both catalyst development and the development of new more advanced equipment.

Two new novel technologies for methanol synthesis have been reported in the literature (Öztürk et al., 1988; Kuczynski et al., 1987a,b; Westerterp and Kuczynski, 1987). The first type involves liquid-phase methanol synthesis in a slurry reactor (Öztürk et al., 1988). This type of reactor is claimed to offer the advantages of easy temperature control and the absence of diffusional resistances. In contrast the quench type fixed-bed methanol converter, for example, is reported to have a catalyst effectiveness factor of 0.5–0.7 as a result of diffusional limitations (Öztürk et al., 1988). The second type of novel methanol reactor is the gas–solid trickle-flow reactor (GSTF) and, its variant, the gas–solid–solid trickle-flow reactor (GSSTFR) (Kuczynski et al., 1987a,b; Westerterp and Kuczynski, 1987). This type of reactor is reported to be advantageous for heterogeneously catalyzed equilibrium gas reactions by shifting equilibrium in a favorable direction by removal of reaction products. However, the GSTF and GSSTFR reactor types have the disadvantage of the presence of pore diffusion limitations.

In this paper, a fluidized-bed configuration for methanol synthesis is presented. Fluidized-bed technology for heterogeneous reversible reactions has the following advantages (Elnashaie and Adris, 1989; Elnashaie et al., 1991).

(i) The problem of pore diffusion resistances is largely eliminated because of the small catalyst pellet sizes used. Industrial fixed-bed pellets are of the order of 6–12-mm diameter, whereas fluidizable catalyst particles can be smaller than 100 μm.

(ii) The equilibrium limitations induced by the reversibility of the reaction(s) are broken. The reactions involved in the methanol synthesis by catalytic hydrogenation of carbon monoxide and carbon dioxide are

$$CO + 2H_2 \rightleftharpoons CH_3OH \quad (1)$$

$$CO_2 + H_2 \rightleftharpoons CO + H_2O \quad (2)$$

$$CO_2 + 3H_2 \rightleftharpoons CH_3OH + H_2O \quad (3)$$

In a fixed-bed reactor, CH_3OH and H_2O production slows down the rate of reaction as equilibrium is approached. In a fluidized-bed reactor almost all of these reactions occur in the dense phase, which contains the catalyst particles (see Figure 1). The bubble phase is almost devoid of catalyst particles. The concentration gradients generated between the two phases due to depletion of reactants and synthesis of products induce the diffusion of CH_3OH and H_2O from the dense phase to the bubble phase and that of CO_2 in the opposite direction. The direction of diffusion of CO depends on the relative rates of reactions 1 and 2. The removal of CH_3OH and H_2O from the gaseous reaction mixture in the dense phase has an effect similar to the removal of CH_3OH by adsorption to the fine solids stream in the gas–solid–solid trickle filter. The rate of reaction and reactants conversion are enhanced due to the reduction in the rate(s) of the reversible reaction(s). As an extreme, a situation can arise where equilibrium conversion is exceeded.

In order to have a realistic comparison with industrial fixed-bed reactors, the same operating conditions of an actual industrial quench-cooled reactor are used to simulate the performance of the suggested fluidized-bed reactor.

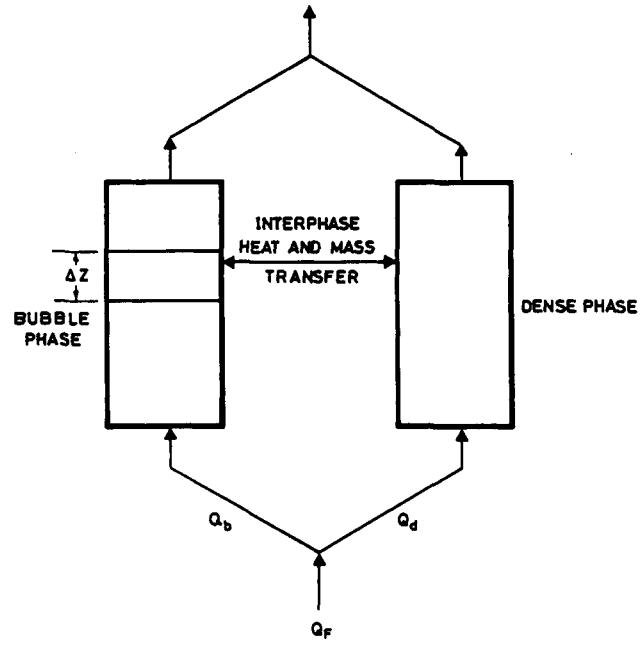

Figure 1. Cross section of bubble and dense phases.

2. Fluidized-Bed Model Description

2.1. Model Assumptions. (i) The dense phase is perfectly mixed, and the bubble phase is in plug flow.

(ii) The bubble phase is devoid of catalyst particles, and all reactions occur in the dense phase.

(iii) The volumetric flow rate of the gas mixture in the dense phase varies with the change in the number of moles due to reaction as well as temperature. The bubble-phase volumetric flow rate is constant (Wagialla et al., 1991).

(iv) The effective bubble size is that at 40% of bed height (Fryer and Potter, 1972).

2.2. Reaction Kinetics. The literature contains several recent publications that describe the kinetics of methanol production from carbon monoxide, carbon dioxide, and hydrogen (Klier et al., 1982; Mcneil et al., 1989; Kuczynski et al., 1987a,b; Graaf et al., 1986; Takagawa and Ohsugi, 1987; Berty et al., 1987). Reactions 1–3 are not stoichiometrically independent, and the methanol production from syngas has been described by various combinations of these reactions. In some studies it has been assumed that methanol is exclusively synthesized from CO and H_2 only (Fryer and Potter, 1972; Mcneil et al., 1989; Kuczynski et al., 1987a,b). There is some disagreement in the literature regarding the role of CO_2. Some investigators postulated that methanol is synthesized from reactions 1 and 2 only and CO_2 acts merely as a catalyst promoter (Villa et al., 1985; Klier et al., 1982). Recently it has been reported that CO_2 does in fact contribute directly to methanol synthesis via reaction 3 (Mcneil et al., 1989; Takagawa and Ohsugi, 1987).

In this paper, the kinetic results reported by Takagawa and Ohsugi (1987) have been used to simulate the reaction rates for methanol synthesis from CO, CO_2, and H_2 over a copper–zinc-based catalyst. These kinetics were selected because they successfully simulated the fixed-bed quench type converter used in this study as a basis for comparison against fluidized-bed reactor (Yahia and Soliman, 1990).

Table I. Parameter Estimates of the Rate Expressions

$a_1 = 2.5, \quad a_2 = 0.35, \quad b = 0.8$
$k_1 = 1.03 \times 10^7 \exp(-16.6/RT)$
$k_2 = 1.25 \times 10^{12} \exp(-28.8/RT)$
$k_3 = 2.33 \times 10^7 \exp(-15/RT)$
$K_{CO_2} = 1.86 \times 10^{-9} \exp(18.1/RT)$
$K_{H_2O} = 1.06 \times 10^{-7} \exp(16.7/RT)$

The rate equations are given by Takagawa and Ohsugi (1987)

$$r_1 = k_1(f_{CO}f_{H_2}^{a_1})^{a_2}\{1 - (f_{CH_3OH}/K_1 f_{CO}f_{H_2}^2)^b\}/(1 + K_{CO_2}f_{CO_2} + K_{H_2O}f_{H_2O}) \quad (4)$$

$$r_2 = k_2 f_{H_2}(1 - f_{CO}f_{H_2O}/K_2 f_{CO_2}f_{H_2}) \quad (5)$$

$$r_3 = k_3 f_{CO_2}(1 - f_{CH_3OH}f_{H_2O}/K_3 f_{CO_2}f_{H_2}^2)/(1 + K_{H_2O}f_{H_2O}) \quad (6)$$

where r_i is the rate of reaction i in moles per liter hour and k_1, k_2, and k_3 are the rate constants of reactions 1–3, respectively. K_{CO_2} and K_{H_2O} are adsorption equilibrium constants of CO_2 and H_2O, respectively; a_1, a_2, and b are constants. The parameter estimates are shown in Table I. Temperature is in kelvin, and R is 1.987 cal/(g-mol K).

The equilibrium constants K_1 and K_3 were obtained as functions of temperature from Klier et al. (1982) as follows:

$$K_1 = \frac{3.27 \times 10^{-13} \exp(11678/T)}{1 - (1.95 \times 10^{-4} \exp(1703/T))P} \quad (7)$$

$$K_3 = [3.826 \times 10^{-11} \exp(6851/T)]/[1 - (1.95 \times 10^{-4}(\exp(1703/T))P)(1 - (4.24 \times 10^{-4}(\exp(1107/T))P))] \quad (8)$$

where T is in kelvin and P in atm.

K_2 is obtained from K_1 and K_3 by the equilibrium relationship

$$K_2 = K_3/K_1 \quad (9)$$

2.3. Model Equations. The steady-state material balance for component j in the bubble phase is

$$\frac{dN_{jb}}{dz} = (K_{bd})_{jb}\left(\frac{N_{jd}}{Q_d} - \frac{N_{jb}}{Q_b}\right)A_b \quad (10)$$

Similarly an energy balance gives

$$\rho_g C_{pg} u_b \frac{dT_b}{dz} = (H_{bd})_b(T_d - T_b) \quad (11)$$

The material balance for the jth component around the dense phase is given by

$$N_{jd} = N_{jdF} + \int_0^H (K_{bd})_{jb}\left(\frac{N_{jb}}{Q_b} - \frac{N_{jd}}{Q_d}\right)A_b\, dz + V(1-\delta)(1-\epsilon)\rho_p \sum_{i=1}^{3} \alpha_{ij} r_i \quad (12)$$

Solving the integral in eq 12 analytically using eq 10, we obtain after some mathematical manipulations

$$N_{jd} = N_{jdF} + u_b A_b\left(\frac{N_{jF}}{Q_F} - \frac{N_{jd}}{Q_d}\right)(1 - e^{-\alpha_j H}) + V(1-\delta)(1-\epsilon)\rho_p \sum_{i=1}^{3} \alpha_{ij} r_i \quad (13)$$

where

$$\alpha_j = \frac{(K_{bd})_{jb}}{u_b}$$

In a similar manner, the dense-phase energy balance for adiabatic operation is

$$\rho_g C_{pg} Q_{dF}(T_F - 298) - \rho_g C_{pg} Q_d(T_d - 298) + \int_0^H (H_{bd})_b(T_b - T_d)A_b\, dz + V(1-\delta)(1-\epsilon)\rho_p \sum_{i=1}^{3}(-\Delta H_i) r_i = 0 \quad (14)$$

Upon integration of eq 11, we obtain

$$T_b = T_d - (T_d - T_F)e^{-\beta z} \quad (15)$$

where

$$\beta = \frac{H_{bd}}{u_b \rho_g C_{pg}}$$

Substituting eq 15 in 14, integrating, and rearranging, we obtain

$$\rho_g C_{pg} Q_{dF}(T_F - 298) - \rho_g C_{pg} Q_d(T_d - 298) + u_b \rho_p C_{pg} A_b (T_F - T_d)(1 - e^{-\beta H}) + V(1-\delta)(1-\epsilon)\rho_p \sum_{i=1}^{3}(-\Delta H_i) r_i = 0 \quad (16)$$

The relevant hydrodynamic and transport property correlations are given in Table II.

The lack of published correlations at the high pressure inside a methanol converter (88 atm in this study) necessitated a literature search to find out how the hydrodynamics inside a fluidized bed may vary with pressure and how such changes would affect converter performance. Several researchers carried out experimental studies at relatively high pressure (Barreto et al., 1983; Rowe et al., 1983; Hoffmann and Yates, 1986; Martin, 1984; Chitester et al., 1984; Jacob and Weimer, 1988, 1987); however their experiments were carried out at pressures well below 23.58 $\times 10^3$ kPa.

There are conflicting reports in the literature regarding the effect of pressure on the voidage at minimum fluidization (ϵ_{mf}) (Jacob and Weimer, 1987; Richardson, 1971; Rowe et al., 1982). Yang et al. (1985) carried out experimental work on particles of sizes ranging from 88 to 3376 μm and at pressures up to 6300 kPa and temperatures up to 1123 K and concluded that the voidage at minimum fluidization does not change appreciably with the change in temperature and pressure. Jacob and Weimer (1987) studied particulate expansion and the minimum bubbling parameters, minimum bubbling velocity (U_{mB}), and bed voidage at minimum bubbling (ϵ_{mB}) for fine carbon powders (d_p = 44 and 112 μm) fluidized with synthesis gas at pressures within the range 2070–12 420 kPa and reported that deviations between minimum bubbling (U_{mB} and ϵ_{mB}) and minimum fluidization (U_{mf} and ϵ_{mf}) conditions increase slightly with increasing pressure.

Saxena and Vogel (1977), using particles of 765-μm diameter at a maximum pressure of 834 kPa, and Rowe et al. (1983), using powders of 262- and 450-μm diameter at pressure up to 6400 kPa, concluded independently that U_{mf} decreases with pressure and follows the original Ergun correlation.

Several investigators (Subzwari et al., 1978; Rowe et al., 1980, 1982) reported that when fine light powders (Geldart Group A) are fluidized in a pressurized vessel, bubbles are smaller and/or fewer in number than when the bed is operated at atmospheric pressure. It has also been reported that as pressure increases, more gas flows in bubble wakes than in bubble voids (Barreto et al., 1983). The same research workers (Barreto et al., 1983) have shown that, for particles of 1.26 g/cm^3 density and 97.7-μm di-

Table II. Hydrodynamic and Transport Property Correlations

parameter	theoretical or empirical expression	ref
superficial velocity at minimum fluidization	$U_{mf} = 0.01(\mu/\rho_g d_p)[(27.2^2 + 0.0408\mathrm{Ar})^{1/2} - 27.2]$ where $\mathrm{Ar} = \rho_g(\rho_p - \rho_g)g(d_p^3/\mu^2)$	Grace, 1986
bubble diameter	$d_B = d_{BM} - (d_{BM} - d_{BO})\exp(-0.3z/D)$ where $d_{BM} = 411.38[A(U_0 - U_{mf})]^{0.4}$, $d_{BO} = 0.376(U_0 - U_{mf})^2$	Mori and Wen, 1975
volume fraction of bubble phase to overall bed	$\delta = (U_0 - U_{mf})/U_b$	Kunii and Levenspiel, 1977
bed voidage at minimum fluidization	$\epsilon_{mf} = 0.586(1.0/\mathrm{Ar})^{0.029}(\rho_g/\rho_p)^{0.021}$	Broadhurst and Becker, 1975
bubble rising velocity	$U_b = U_0 - U_{mf} + (gd_B)^{0.5}$	Kunii and Levenspiel, 1977
total feed volumetric velocity	$Q_F = U_0 A$	Kunii and Levenspiel, 1977
bubbles volumetric flow rate	$Q_B = (U_0 - U_{mf})\,A$	Kunii and Levenspiel, 1977
dense phase feed volumetric flow rate	$Q_{dF} = Q - Q_B$	Kunii and Levenspiel, 1977
expanded bed height	$H = H_{mf}/(1 - \delta)$	Kunii and Levenspiel, 1977
overall mass-transfer coefficient (bubble phase–dense phase) based on bubble volume	$(K_{bd})_{jb} = \frac{U_{mf}}{3} + [(4D_{jm}\epsilon_{mf}U_b/\pi d_B)]^{1/2}$	Sit and Grace, 1978
diffusivity of component j in gas mixture	$D_{jm} = (1 - x_j)/(\sum_{\substack{i=1 \\ i\neq j}}^{n} (x_j/D_{ji}))$	Reid et al., 1977
binary diffusivity	$D_{ij} = 0.04357\frac{T^{3/2}}{P(V_i^{1/3} + V_j^{1/3})^2}\left[\frac{1}{M_i} + \frac{1}{M_j}\right]^{1/2}$	Coulson and Richardson, 1965
overall heat-transfer coefficient (bubble phase–dense phase) based on bubble volume	$\frac{1}{(H_{bd})_b} = \frac{1}{(H_{bc})_b} + \frac{1}{(H_{cd})_b}$ where $(H_{bc})_b = 4.5(U_{mf}\rho_g C_{pg}/d_B) + 0.104(K_g\rho_g C_{pg}/d_B^{2.5})^{1/2}$, $(H_{cd})_b = 21.44(K_g\rho_g C_{pg})^{1/2}(\epsilon_{mf}U_b/d_B)^{1/2}$	Kunii and Levenspiel, 1977
heat-transfer coefficient (bed-vertical tubes)	$h_w = 0.88\frac{K_g}{d_p}\mathrm{Ar}^{0.213}$	Renz et al., 1987

ameter, the equivalent bubble diameter decreased from 4 to 2 cm (a decrease of 50%) as pressure was increased from 208.65 to 1251.9 kPa.

2.4. Industrial Methanol Converter Design and Operating Data. Figure 2 shows a drawing of the quench-cooled methanol converter used in this investigation as a basis for comparison between fixed- and fluidized-bed processes for methanol synthesis. The flow and design data of this converter are given in Table III.

2.5. Solution Techniques: 2.5.1. Equilibrium Conversions. Since only two reactions among reactions 1–3 are stoichiometrically independent, any two components in the gaseous reaction mixture are sufficient to describe the system and obtain the concentrations of other mixture species. In the present investigation CO and H_2 are chosen as the key components. Let

$$X_{CO} = \frac{\text{moles of CO reacted}}{\text{moles of CO in feed}} \quad (17)$$

$$X_{H_2} = \frac{\text{moles of } H_2 \text{ reacted}}{\text{moles of CO in feed}} \quad (18)$$

$$X_1 = \frac{\text{moles of CO reacted in reaction 1}}{\text{moles of CO in feed}} \quad (19)$$

$$X_2 = \frac{\text{moles of } CO_2 \text{ reacted in reaction 2}}{\text{moles of CO in feed}} \quad (20)$$

$$X_3 = \frac{\text{moles of } CO_2 \text{ reacted in reaction 3}}{\text{moles of CO in feed}} \quad (21)$$

Stoichiometrically we have the following relationships:

$$X_{CO} = X_1 - X_2 \quad (22)$$

$$X_{H_2} = 2X_1 + X_2 + 3X_3 \quad (23)$$

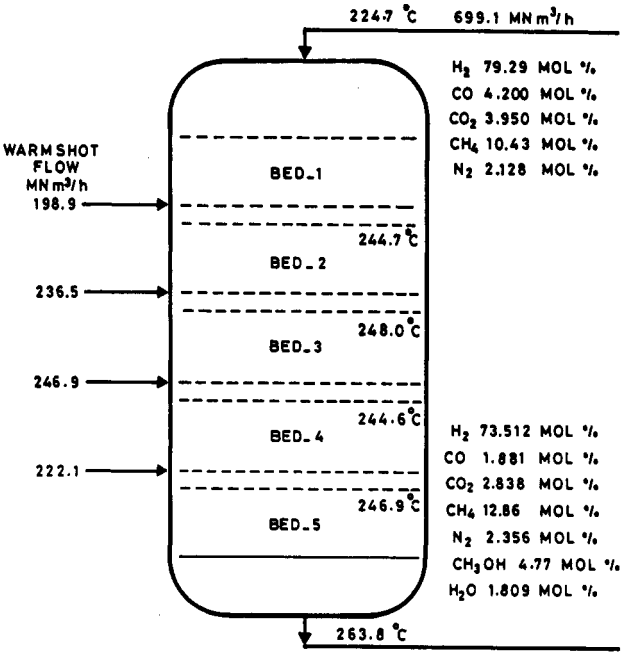

Figure 2. Fixed-bed configuration.

Let n_j and F_j denote feed and exit molar flow rates of component j; thus,

$$n_{CO} = F_{CO}(1 - X_{CO}) \quad (24)$$

$$n_{H_2} = F_{H_2} - X_{H_2}F_{CO} \quad (25)$$

$$n_{CH_3OH} = F_{CH_3OH} + (X_1 + X_3)F_{CO} \quad (26)$$

$$n_{CH_3OH} = F_{CH_3OH} + \left(\frac{X_{CO} + X_{H_2}}{3}\right)F_{CO} \quad (27)$$

$$n_{CO_2} = F_{CO_2} - (X_2 + X_3)F_{CO} \quad (28)$$

$$n_{CO_2} = F_{CO_2} - \left(\frac{X_{H_2} - 2X_{CO}}{3}\right)F_{CO} \quad (29)$$

$$n_{H_2O} = F_{H_2O} + (X_2 + X_3)F_{CO} \quad (30)$$

$$n_{H_2O} = F_{H_2O} + \left(\frac{X_{H_2} - 2X_{CO}}{3}\right)F_{CO} \quad (31)$$

The total number of moles (N_T) is the sum of all component mole fractions

$$N_T = N_{CO} + N_{H_2} + N_{CH_3OH} + N_{CO_2} + N_{H_2O} \quad (32)$$

The mole fraction of component j (x_j) is

$$x_j = \frac{N_j}{N_T} \quad (33)$$

The fugacity of component j (f_j) is

$$f_j = \phi_j x_j P \quad (34)$$

where ϕ_j is the fugacity coefficient of component j (Reid et al., 1977).

The equilibrium conversions of CO and H_2 are calculated by computing X_{CO} and X_{H_2} at which the rates of reactions r_1, r_2, and r_3 are zero. The IMSL routine ZSPOW was used for this purpose.

2.5.2. Steady-State Computations. There are seven species in the reaction mixtures: five reacting species and two inerts. These are CO, H_2, CH_3OH, CO_2, H_2O, N_2, and CH_4. Thus eq 13 constitutes a system of nonlinear equations that are to be solved simultaneously with the energy balance equation (16). The technique used was to decouple the solution of the material balances (system of equations (13)) and the energy balance as follows.

Step 1. Select a dense phase operating temperature and solve the set of equations (13).

Step 2. For the same temperature calculate the heat function (obtained from eq 16) defined as follows:

$$\text{heat function} = \rho_g C_{pg} Q_{dF}(T_F - 298) - \rho_g C_{pg} Q_d(T_d - 298) + u_b \rho_g C_{pg} A_b (T_F - T_d)(1 - e^{-\beta H}) + V(1 - \delta)(1 - \epsilon)\rho_p \sum_{i=1}^{3}(-\Delta H_i) r_i$$

Step 3. Select another dense-phase temperature, and repeat the calculations in step 1 and 2.

Step 4. Repeat step 3 until the temperature range (175–400 °C) is scanned.

Step 5. Plot the heat function data so obtained against temperature. The temperature at which the heat function crosses the zero line (abscissa) represents the steady-state dense-phase temperatures.

The point at which the heat function crosses the zero line can be changed by changing the feed temperature T_F (this shifts the whole heat function curve upward or downward) and/or changing the rate of cooling (or heating) when nonadiabatic operation is employed.

3. Results and Discussions

Carbon monoxide and methanol production rates (based on the combined dense-phase and bubble-phase conditions) are used as performance indices and are defined as follows:

CO conversion (hereafter referred to as conversion) = $\frac{\text{total CO feed to all beds} - \text{CO reacted}}{\text{total CO feed to all beds}}$

CH_3OH production rate = total CH_3OH molar flow rate leaving the reactor (kg-mol/s)

According to reaction 1

$$CO + 2H_2 \rightleftharpoons CH_3OH$$

higher CO conversion results in higher CH_3OH production. Reaction 2

$$CO_2 + H_2 \rightleftharpoons CO + H_2O$$

indicates that some CO is produced, and this CO can be converted to CH_3OH according to reaction 1. Reaction 3

$$CO_2 + 3H_2 \rightleftharpoons CH_3OH + H_2O$$

indicates that some CH_3OH is produced from CO_2 and H_2 (independently from CO availability in the reaction mixture). The relative predominance of the rates of reactions 1 and 3 dictates how closely methanol production matches CO conversion. We found from the computed results that higher CO conversion is very closely related to higher CH_3OH production, indicating that reaction 1 is the predominant reaction for CH_3OH production.

In order to compare the fixed- and fluidized-bed reactors on an equal basis, the catalyst bed weights in each bed as well as the reactant feed rates were maintained the same for both types of reactors.

The flow of gas in the fixed-bed converter is from top to bottom, but in the fluidized-bed converter it has to be of course in the reverse direction, with the top bed in the

Table III. Design and Operating Conditions of the Fixed-Bed Quench-Cooled Reactor

	flow rate, $(nm^3/h) \times 10^{-3}$	temp, °C
fresh feed to bed 1	699.1	224.7
warm shot to bed 2	198.9	224.7
warm shot to bed 3	236.5	224.7
warm shot to bed 4	246.9	224.7
warm shot to bed 5	222.1	224.7

Mole Percentage of Component in Fresh Feed and Cold Shots and in Exit from Bed Number 5

component	composition, mol %: in each fresh feed stream	composition, mol %: in exit stream from bed no. 5
CO	4.2	1.881
H_2	79.29	73.512
CH_3OH		4.744
CO_2	3.95	2.838
H_2O		1.809
N_2	2.128	2.356
CH_4	10.43	12.86

Catalyst Bed Dimensions

	height, m	diameter, m
top dome	1.5	5.88
bed 1	1.625	5.8
bed 2	1.8	5.8
bed 3	1.8	5.8
bed 4	2.1	5.8
bed 5	2.4	5.8

bulk catalyst density	1250 kg/m³
effective static catalyst bed void fraction (Lee et al., 1984)	0.4

Table IV. Operating Parameters in Each of the Five Fluidized Beds

bed no.	bubble diam, cm	expanded bed ht, cm	superficial gas velocity U_0, cm/s	bubble fracn in bed (δ)	optimum dense-phase temp, K
1	1.67	538	20.5	0.35	543
2	1.49	414	24.7	0.42	538
3	1.92	450	31.9	0.46	533
4	2.56	543	38.1	0.48	533
5	3.23	635	44.1	0.49	533

Table V. Effect of Converter Diameter Variation on Its Performance

converter diameter, m	H_{mf}/D for the 5th bed	methanol production rate, g-mol/s	CO conversion, %
3	2.97	1.0068	71.63
4	1.25	1.0121	71.99
5 (base case)	0.642	1.0121	71.98
6	0.372	1.0120	71.98
7	0.234	1.0119	71.97

fixed-bed converter used as the bottom bed in the fluidized-bed configuration.

The cross-sectional area in the fluidized bed was then so chosen that bubbling fluidization is ensured in each bed. The hydrodynamic correlations gave the minimum fluidization velocity (U_{mf}) as 5.26 cm/s. Satisfactory fluidized-bed conditions were obtained for a converter diameter of 5 m in each bed. Table IV summarizes the fluidized-bed converter operating parameters.

The sensitivity of the fluidized-bed-reactor performance to the selection of a 5-m diameter was checked by computing the heat function, methanol production rate, and CO conversion for converters with 3-, 4-, 6- and 7-m diameters. In each case, the converter catalyst weight was maintained constant by changing the bed height. Table V summarizes the results of these computations. From Table V it is clear that variation of H_{mf}/D from 2.97 to 0.234 did not have a significant impact on reactor performance and the production rate increased by only 0.5%. A change of converter diameter results in two opposing trends on reactor performance; for the same feed gas volumetric flow rate, a decrease in reactor diameter (and hence a decrease in the converter cross-sectional area) has the effect of increasing the superficial gas velocity (U_0). This in turn causes an increase in bubble size, which has the negative effect of decreasing the total available area for mass transfer between the dense and bubble phases. On the other hand, a small cross-sectional area (for the same catalyst bed size) results in a deeper bed and hence an increased contact time between reactants and catalyst and therefore improved converter performance. An increase in bed diameter would reverse these two trends.

A parametric sensitivity analysis of the effect of particle diameter (d_p) was also undertaken. In the base case, particle diameter of 300 μm was used. Particle sizes of 200, 400, and 500 μm were then tested, but the system performance regarding production rate and conversion remained unchanged. Particle diameter variation affected the minimum fluidization velocity (U_{mf}). U_{mf} in the fifth bed changed from 5.26 to 9.63 cm/s as d_p was changed from 300 to 500 μm, but U_0 was maintained at 44.1 cm/s. A change in U_{mf} changes the value of the mass-transfer exchange parameter $(K_{bd})_{jb}$. However, as will be explained later, the system is rather insensitive to small changes in $(K_{bd})_{jb}$ for the small bubble sizes used in this study. Very small particle sizes were not used in the simulations because such particles (at a particle density of 1250 kg/m^3) fall in Group C of Geldart classification (Geldart, 1973), which are in practice very difficult to fluidize because interparticle forces have a larger influence on the particles than the gravitional force and therefore the gas passes through channels in the bed (Howard, 1989).

Table VI. Effect of Changes in $(K_{bd})_{jb}$ Values on Converter Performance (Small Bubble Size)

$(K_{bd})_{jb}$ values	CH_3OH production rate, g-mol/s	CO conversion, %
unchanged	1.0121	71.98
$(K_{bd})_{jb} = 0$	0.4688	33.68
reduced by 25%	1.0121	71.98
reduced by 50%	1.0121	71.98
reduced by 75%	1.0103	71.86
increased by 25%	1.0121	71.98
increased by 50%	1.0121	71.98

Table VII. Effect of Changes in $(K_{bd})_{jb}$ Values on Converter Performance (Large Bubble Size)

$(K_{bd})_{jb}$ values	CH_3OH production rate, g-mol/s	CO conversion, %
unchanged	0.9865	70.16
reduced by 20%	0.9729	69.19
reduced by 40%	0.9493	57.50
reduced by 60%	0.9042	64.27
reduced by 80%	0.8007	56.90
$(K_{bd})_{jb} = 0$	0.4684	33.66
increased by 20%	0.9949	70.76
increased by 40%	1.0002	71.14
increased by 60%	1.0037	71.39
increased by 80%	1.0061	71.56
increased by 100%	1.0076	71.67

Since the estimated values of the mass-transfer coefficients $(K_{bd})_{jb}$ have an important effect on the performance of the converted, a sensitivity analysis on the estimated $(K_{bd})_{jb}$ values was carried out, and the results are shown in Table VI. A negative change in $(K_{bd})_{jb}$ values as large as 75% did not change the results to any appreciable extent. This insensitivity is due to the fact that relatively small bubble sizes were used in the study. Small bubble sizes were used in the study because it has been generally agreed by several research workers that high-pressure operation is expected to result in smaller bubble sizes (Barreto et al., 1983; Rowe et al., 1980, 1982, 1983; Subzwari et al., 1978). When large bubble sizes are used (in the order of 200 cm), the system becomes quite sensitive to changes in $(K_{bd})_{jb}$, as shown in Table VII. A reduction in the $(K_{bd})_{jb}$ values by 40%, for example, can reduce the methanol production rate by 3.8%.

The fluidized-bed-converter adiabatic operation was optimized in such a way that the output from each bed was at the dense-phase temperature that corresponds to the maximum methanol production rate in that bed. The exit stream was then mixed with the syngas warm shot. The gas mixture temperature was then adjusted (by cooling or heating) so that the steady-state dense-phase temperature of the subsequent bed (which is found at the intersection of the heat function plot with the zero line) corresponds to the maximum methanol production rate.

Figures 3 and 4 show the plots of conversion, production rate, and heat function versus dense-phase temperature for the first and fifth beds of the fluidized beds, respectively. The operating dense-phase temperature in the first bed should be about 535 K in order for the system to operate at optimum conditions of conversion and methanol production rate. To achieve this steady state, the feed temperature to the first bed should be 423 K and not the fixed-bed feed temperature of 497.7 K (224.7 °C). In selecting this feed temperature, a bifurcation analysis was

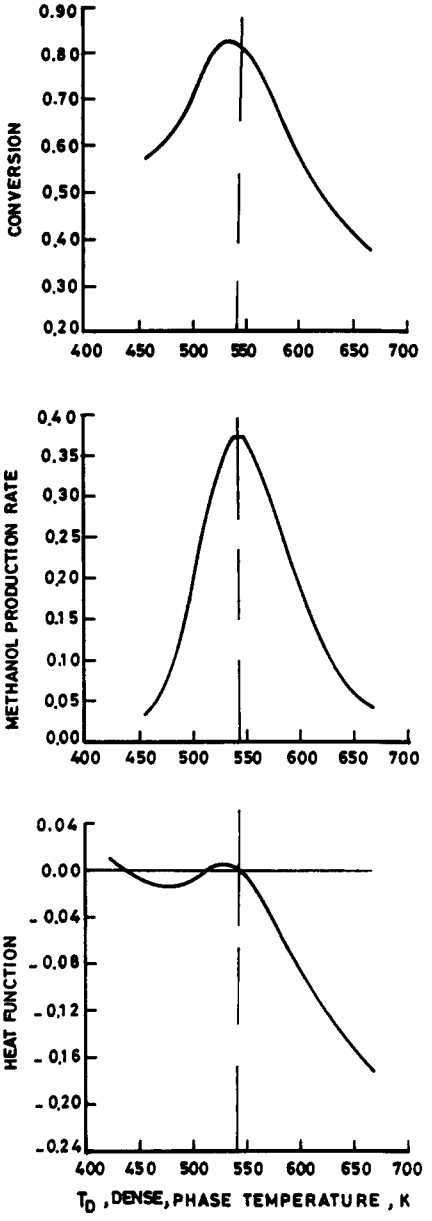

Figure 3. Conversion, production rate, and heat function vs T_D for the first fluidized bed.

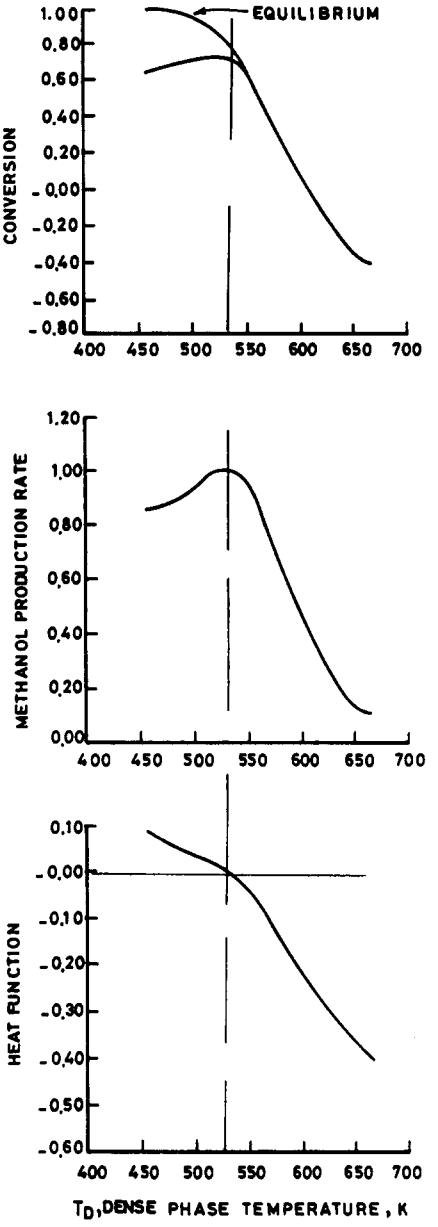

Figure 4. Conversion, production rate, and heat function vs T_D for the fifth fluidized bed.

undertaken to ascertain the existence and location of multiple steady states. Figure 5 shows the hysteresis plot of the dense-phase temperature (T_D) versus feed temperature (T_F) for the first fluidized bed. Point A on this plot corresponds to the fixed-bed feed temperature of 497.7 K. A single steady state exists at this point and is of course a stable steady state, but at this temperature optimum operation is not realized.

The optimum conditions are obtained when T_D = 535 K, as shown in Figure 3. The hysteresis curve of Figure 5 shows that this dense-phase operating temperature corresponds to point B and the corresponding feed temperature should be 423 K. However at a feed temperature of 423 K two other steady states (at points C and D) exist. Point D corresponds to an extinction temperature, and the middle point C is an unstable steady state. Point B is a stable steady state. Figure 4 indicates the fifth bed and thus the overall performance of the converter. The sharper peak of the methanol production rate curve shows that it is a more accurate performance index than the relatively flatter conversion curve. Operation at a dense-phase temperature in the fifth bed of 528 K would maintain a maximum production rate of 1.0121 kg-mol/s (or about 2800 MTPD (MTPD is metric ton per operating day)) at an overall conversion of about 72%.

Operating at temperatures exceeding 565 K would maintain conversion at its equilibrium level. In contrast, the fixed-bed converter had a methanol production rate of 0.787 kg-mol/s (or about 2175 MTPD) and an overall conversion of only 63.06%. Thus fluidized-bed usage represents a 28.6% improvement in the methanol production rate over that with the fixed bed.

The superior performance of the fluidized bed is due to the following advantages over the fixed-bed counterpart.

(i) For the smaller size of the catalyst pellets in the fluidized bed (d_p = 300 μm), the effectiveness factor is unity. Mass- and heat-transfer pore diffusional resistances can reduce the effectiveness factor in a fixed bed to 0.5–0.7 (Kuczynski et al., 1987a,b). Smaller pellet sizes cannot be used in fixed beds because an excessive pressure drop can build up in the converter.

(ii) As the reaction proceeds in the dense phase, the accumulation of products (CH_3OH, H_2O, and, to a lesser extent, CO) creates concentration gradients between the dense and bubble phases. Diffusion of reaction products

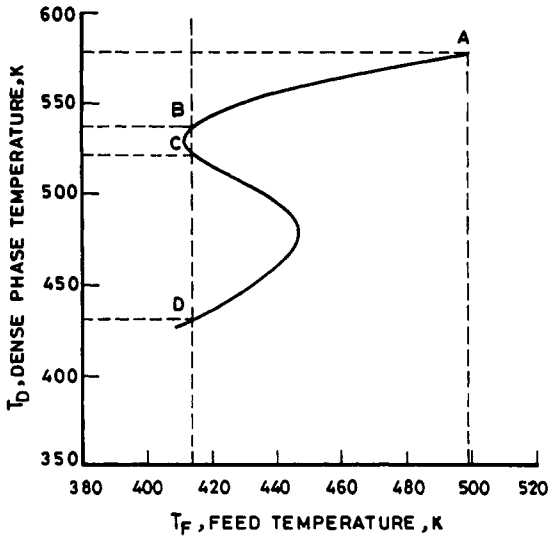

Figure 5. Bifurcation plot of T_d vs T_F for the first fluidized bed.

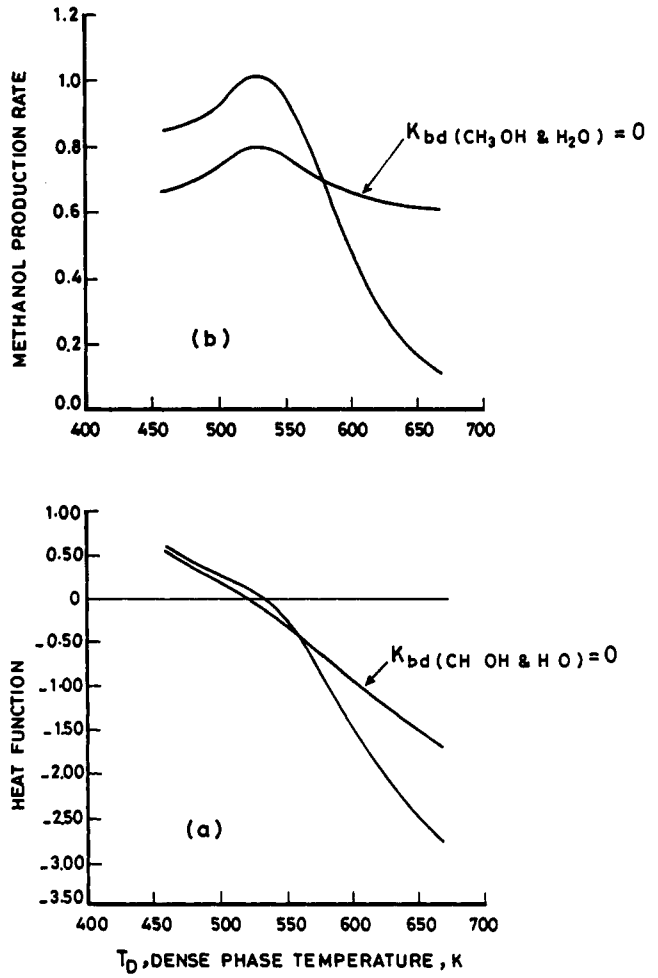

Figure 6. Production rate and heat function vs T_D; effect of $(K_{bd})_{CH_3OH} = 0$ and $(K_{bd})_{H_2O} = 0$ simultaneously.

from the dense phase into the bubble phase shifts the reaction to the right and limits the incidence of the reversible reaction, which decomposes methanol, with an attendant improvement in conversion and methanol production rate. Thus the bubble/dense interphase acts as a natural membrane for selectively removing the reaction products.

(iii) The isothermality of the fluidized bed is advantageous for optimum operating conditions in contrast to the temperature profile that exists in fixed beds and corresponds to a continuous change in the plug flow type operating conditions along the length of the converter.

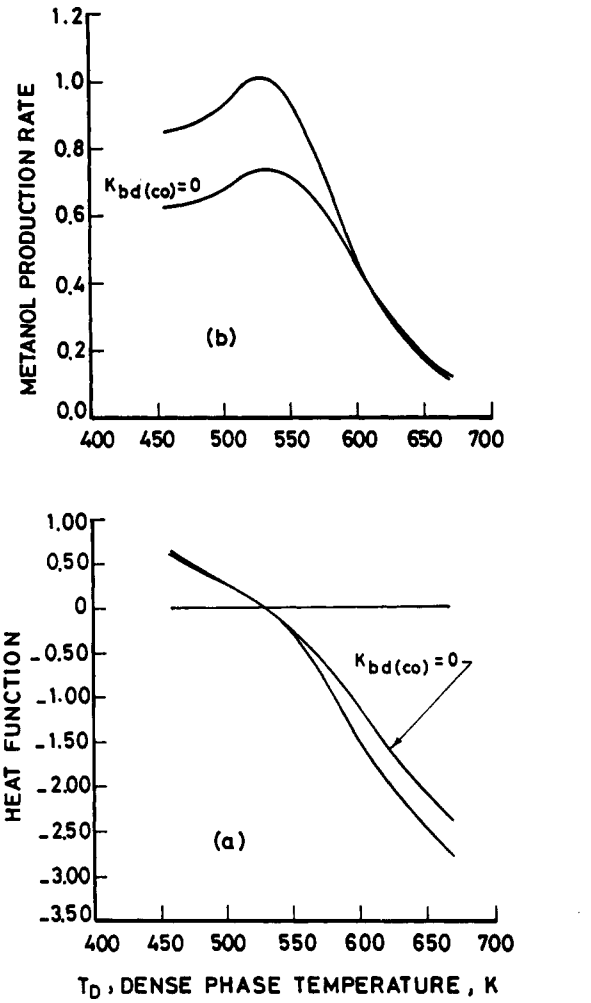

Figure 7. Production rate and heat function; effect of $(K_{bd})_{CO} = 0$.

To obtain an estimate for the impact of the diffusion of the reaction products between the dense and bubble phases on methanol production rate, the diffusion of CH_3OH and/or H_2O were artificially suppressed (by setting the relevant $(K_{bd})_{jb} = 0$). The effect of these simulations are shown in Figures 6–8. As shown in Figure 6, suppression of the interphase diffusion of both CH_3OH and H_2O reduces the maximum CH_3OH production rate from about 1.0 to about 0.78 kg-mol/s. This is because the confinement of the products of reaction (CH_3OH and H_2O) to the active dense phase increases the rate of the backward reaction rate and thus reduces the production rate of CH_3OH from the overall reaction. At temperatures above about 585 K, this trend is reversed because at such high temperatures the dominant reaction rate is the backward rate and CH_3OH is being decomposed rather than synthesized. Figure 7 indicates that the suppression of CO diffusion reduces the maximum CH_3OH production rate from about 1.0 to about 0.72 kg-mol/s, which is a more pronounced effect than that of the suppression of the diffusion of CH_3OH and H_2O shown earlier in Figure 6. This is because reaction 1 in which CH_3OH is synthesized from CO and H_2

$$CO + 2H_2 \rightleftharpoons CH_3OH \qquad (1)$$

is a faster reaction than reaction 2 in which the role of CO is a product role

$$CO_2 + H_2 \rightleftharpoons CO + H_2O \qquad (2)$$

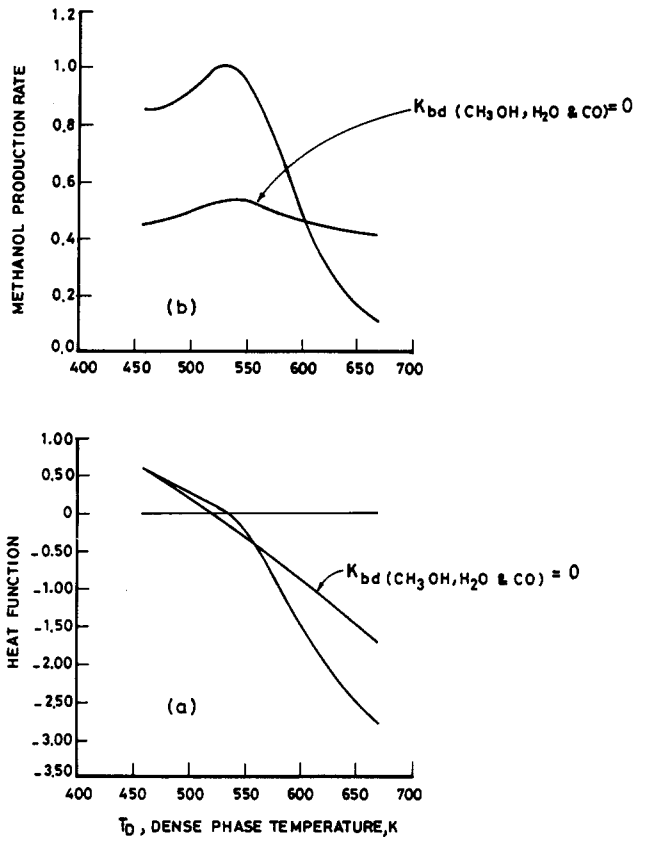

Figure 8. Production rate and heat function vs T_D; effect of $(K_{bd})_{CH_3OH} = 0$, $(K_{bd})_{H_2O} = 0$, and $(K_{bd})_{CO} = 0$ simultaneously.

Thus suppression of the diffusion of the reactant CO from the bubble phase to the dense phase deprives reaction 1 of an important reactant, and the forward reaction rate is reduced and subsequently CH_3OH production rate is diminished. The combined effect of the suppression of the interphasial diffusion of CH_3OH, H_2O, and CO is demonstrated in Figure 8, where a very large decrease in the maximum methanol production rate from about 1.0 to about 0.52 kg-mol/s occurs.

One of the disadvantages of fluidized-bed converters is that back-mixing in the active dense phase reduces conversion. To overcome this disadvantage, the converter may be divided into a number of beds in series. Such a division makes the converter operation resemble plug flow operation with an attendant increase in overall conversion. To obtain a measure of CH_3OH production rate improvement for such configurations, the total converter volume is divided into 10 equally sized beds, as shown in Figures 9 and 10. In Figure 9 the total fresh feed is divided into 10 equally sized streams, and thus each bed is fed with the same rate of fresh feed (in addition to the feed from the exit stream of the previous bed). In Figure 10 all the fresh feed is fed to the first bed. Figure 10 shows that such an arrangement results in a maximum CH_3OH production of 1.178 kg-mol/s (i.e. about 3257 MTPD) at an overall conversion of 86%. However operation of 10 fluidized beds in series is not an easy technical undertaking, and it would be interesting to see the simulation results of operation at the other extreme, i.e. operation of the entire methanol converter as a single bed. This is shown in Figure 11. Here the production rate of CH_3OH at its maximum is 0.9596 kg-mol/s (corresponding to about 2644 MTPD) at a conversion of 68.2%. In comparing the single-fluidized-bed converter against the five-fixed-beds configuration it is interesting to note that even the single-fluidized-bed reactor turns out to be more efficient, since the fixed-bed

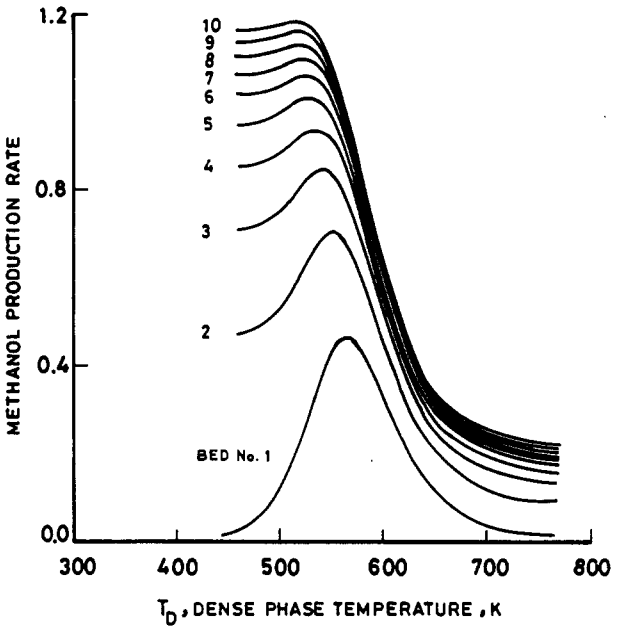

Figure 9. Production rate vs T_D with the fluidized bed divided into 10 equally sized beds.

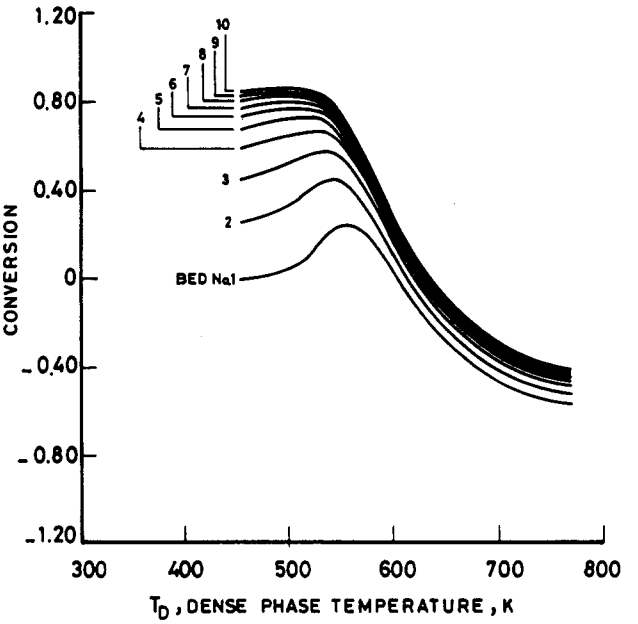

Figure 10. Conversion vs T_D with the fluidized bed divided into 10 equally sized beds.

CH_3OH production rate was only 2175 MTPD.

4. Conclusions

This preliminary theoretical investigation has shown that fluidized-bed technology is more efficient for methanol synthesis than the conventional fixed-bed technology. On the basis of the same converter bed arrangement, the fluidized-bed setup resulted in a CO conversion of about 72%, while the actual fixed-bed CO conversion is 63.06% only. The fluidized bed gives a methanol production rate of 1.0121 kg-mol/s while the fixed-bed production rate is 0.778 kg-mol/s. This represents a percentage improvement in methanol production rate of about 30%. Operation of the fixed-multibed methanol converter as a single fluidized bed proved also more advantageous with a CO conversion of 68.2% and a methanol production rate of 0.9596 kg-mol/s. As an extreme, operation of the fluidized-bed

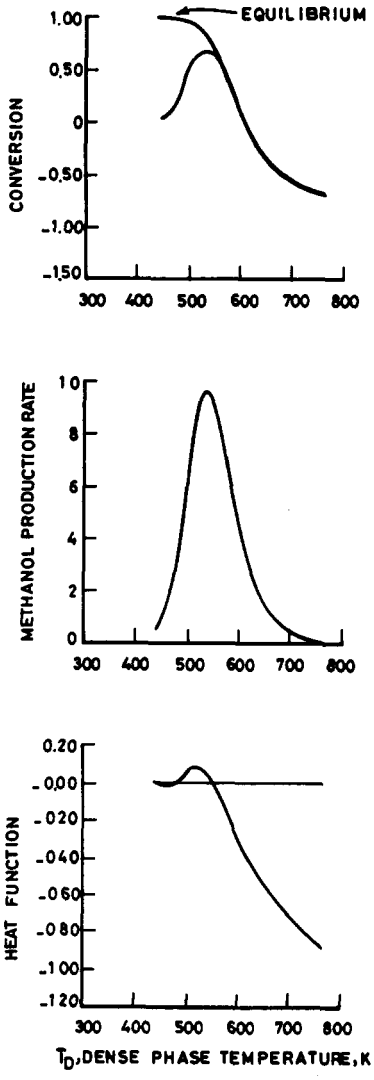

Figure 11. Conversion, production rate, and heat function for fluidized bed as a single large bed.

configuration as 10 equally sized fluidized beds in series gave a CO conversion of 86% and a methanol production rate of 1.178 kg-mol/s, which represents a 51.1% increase in production rate over the conventional five-fixed-beds quench type converter.

This preliminary theoretical investigation points very clearly to the great advantages that may be achieved through using a fluidized-bed rather than a fixed-bed configuration for the catalytic production of methanol. Much experimental and theoretical work is needed in order to realize this exciting possibility practically.

Nomenclature

A_b = cross-sectional area of the bubble phase, m^2
C_{pg} = gas heat capacity, J/(kg K)
D = converter diameter, m
D_{jm} = diffusivity of component j in gas mixture, $m^2\ s^{-1}$
d_B = bubble diameter, m
d_p = particle diameter, m
f_j = fugacity of component j, atm
g = gravitational acceleration, m/s^2
H = expanded bed height, m
H_{mf} = bed height at minimum fluidization conditions, m
h = time, h
$(H_{bd})_b$ = interphase heat-transfer coefficient between bubble and dense phases based on bubble volume, J/(m^3 s K)
K_1, K_2, K_3 = equilibrium constant of reactions 1–3, respectively
k_1, k_2, k_3 = rate constants of reactions 1–3, respectively
K_g = thermal conductivity of gas, J/(K·m·s)
$(K_{bd})_{jb}$ = interphase mass-transfer coefficient between bubble and dense phases based on bubble volume, s^{-1}
N_j = molar flow rate of component j leaving reactor, kmol/s
N_{jb} = molar flow rate of component j in the bubble phase, kmol/s
N_{jd} = molar flow rate of component j in the dense phase, kmol/s
N_{jF} = molar flow rate of component j in fresh feed to fluidize bed reactor, kmol/s
N_{jdF} = molar flow rate of component j at the inlet of the dense phase, kmol/s
P = reactor pressure, atm
Q_F = volumetric flow rate of total feed to reactor, m^3/s
Q_b = volumetric flow rate of bubble phase gas, m^3/s
Q_d = volumetric flow rate of exit dense-phase gas, m^3/s
Q_{dF} = volumetric flow rate of inlet dense phase, m^3/s
r_i = rate of reaction i, (mol/L)/h
T_b = bubble-phase temperature, K
T_d = dense-phase temperature, K
T_F = feed gas temperature, K
U_b = superficial gas velocity of bubble-phase gas, m/s
U_0 = superficial gas velocity fresh feed gas, m/s
U_{mf} = superficial gas velocity of fresh feed gas at minimum fluidization, m/s
V = volume of overall reactor, m
x_j = mole fraction of component j
z = distance along bed height, m
δ = bubble-phase volume as a fraction of total bed volume, dimensionless
ϕ_j = fugacity coefficient of component j
ΔH_i = heat or reaction i, J/g-mol
ρ_g = density of gas, kg/m^3
ρ_p = densities of solid particles, kg/m^3
ϵ_{mf} = dense-phase voidage at minimum fluidization conditions, dimensionless
μ = viscosity, kg/(m s)

Registry No. CO, 630-08-0; CH_3OH, 67-56-1; CO_2, 124-38-9.

Literature Cited

Barreto, G. F.; Yates, J. G.; Rowe, P. N. The effect of pressure on the flow of gas in fluidized beds of fine particles. *Chem. Eng. Sci.* **1983**, *38*, 1935–1945.

Berty, J. M.; Lee, S.; Sivagnanam; Szeifert, F. Diffusional kinetics of catalytic vapour phase reversible reactions with decreasing total number of moles. *Inst. Chem. Eng. Symp. Ser.* **1987**, 87.

Broadhurst, T. E.; Becker, H. A. Onset of fluidization in slugging beds of uniform particles. *AIChE J.* **1975**, *21*, 238–247.

Chitester, D. C.; Kornosky, R. M.; Fan, L.; Danko, J. P. Characteristics of fluidization at high pressure. *Chem. Eng. Sci.* **1984**, *39*, 253–261.

Coulson, J. M.; Richarson, J. F. *Chemical Engineering*; Pergamon Press: New York, 1965; Vol. 1.

Elnashaie, S. S. E. H.; Adris, A. M. A fluidized bed steam reformer for methane. *Proceeding of the International Conference on Fluidization, Fluidization VI*; Grace, J. R., Shemilt, L. W., Bergougnou, M. A., Eds.; Banff; May 1989; pp 319–326.

Elnashaie, S. S. E. H.; Wagialla, K. M.; Abashar, M. M. E. The use of mathematical models to explore the applicability of fluidized bed technology to thermodynamic/diffusion limited reversible catalytic reactions. Ammonia Synthesis. *Math. Comput. Modell.* **1991**, in press.

Fryer, C.; Potter, O. E. Bubble size variation in two phase models of fluidized bed reactor. *Powder Technol.* **1972**, *6*, 317–322.

Geldart, D. Types of gas fluidization. *Powder Technol.* **1973**, *7*, 285–292.

Graaf, G. H.; Sijtsema, P. J. J. M.; Stamhuis, F. J.; Joosten, G. E. H. Chemical equilibria in methanol synthesis. *Chem. Eng. Sci.* **1986**, *41*, 2883–2890.

Graff, G. H.; Scholtens, H.; Stamhuis, E. J.; Beenackers, A. A. C. M. Intraparticle diffusion limitations in low-pressure methanol synthesis. *Chem. Eng. Sci.* **1990**, *45*, 773–783.

Grace, J. R. Modelling and simulation of two-phase fluidized bed reactors. *Chemical Reaction Design Technology*; NATO ASI

Series, Series E.; Kluwer: Boston, MA, 1986; Vol. 110, pp 245-289.
Hoffman, A. C.; Yates, J. G. Experimental observations of fluidized beds at elevated pressures. *Chem. Eng. Sci.* **1986**, *41*, 133-149.
Howard, J. R. Fluidized bed technology-principles and applications. Adam Hilger: Bristol, New York, 1989.
Jacob, K. V.; Weimer, A. W. High-pressure particulate expansion and minimum bubbling of fine carbon powders. *AIChE J.* **1987**, *33*, 1698-1706.
Jacob, K. V.; Weimer, A. W. Normal bubbling of fine carbon powders in high-pressure fluidized beds. *AIChE J.* **1988**, *34*, 1395-1397.
Klier, K.; Chatikavanij, V.; Herman, R. G.; Simmons, G. W. Catalytic synthesis of methanol from CO/H_2, IV, the effects of carbon dioxide. *J. Catal.* **1982**, *74*, 343-360.
Kuczynski, M.; Browne, W. I.; Fontein, H. J.; Westerterp, K. R. Reaction kinetics for the synthesis of methanol from CO and H_2 on a copper catalyst. *Chem. Eng. Process.* **1987a**, *21*, 179-191.
Kuczynski, M.; Oyevaar, M. H.; Pieters, R. T.; Westerterp, K. R. Methanol synthesis in a countercurrent gas-solid-solid trickle flow reactor, an experimental study. *Chem. Eng. Sci.* **1987b**, *42*, 1887-1898.
Kunii, D.; Levenspiel, O. *Fluidization Engineering*; Wiley: New York, 1977.
Lee, K. S.; Hong, C. S.; Lee, C. Kinetic modelling and reactor simulation for methanol synthesis from hydrogen and carbon monoxide on a copper base catalyst. *Korean J. Chem. Eng.* **1984**, *1*, 1-11.
Martin, H. The effects of pressure and temperature on heat transfer to gas fluidized beds of solid particles. XVI ICHMT Symposium, Sept 1984, Dubrovmyt, Yugoslavia.
Mcneil, M. A.; Schack, C. J.; Rinker, R. G. Methanol synthesis from hydrogen, carbon monoxide and carbon dioxide over a $CuO/ZnO/Al_2O_3$ catalyst, II, development of a phenomenological rate expression. *Appl. Catal.* **1989**, *50*, 265-285.
Mori, S.; Wen, C. Y. Estimation of bubble diameter in gaseous fluidized beds. *AIChE J.* **1975**, *21*, 109-115.
Öztürk, S. S.; Shah, Y. T.; Decker, W. D. Comparison of gas and liquid phase methanol synthesis processes. *Chem. Eng. J.* **1988**, *37*, 177-192.
Reid, R. C.; Prausnitz, J. M.; Sherwood, T. K. *The properties of gases and liquids*, 3rd ed.; McGraw-Hill: London, 1977.
Renz; et al. Heat transfer characteristics of the FBC Acchen Technical University. *Proceedings of the 1987 International Conference on fluidized bed combustion*; American Society of Melchanical Engineers: New York, 1987.
Richardson, J. F. *Fluidization*; Davidson, J. F., Harrison, D., Eds.; Academic Press: New York, 1971; p 50.
Rowe, P. N.; MacGillivary, H. J. A preliminary X-ray study of the effect of pressure on a bubbling gas-fluidized bed. *Inst. Energy Symp. Ser.* **1980**, *1* (No. 4), IV-1.
Rowe, P. N.; Foscolo, P.; Hoffmann, A. C.; Yates, J. G. Fine powders fluidized at low velocity at pressures up to 20 bar with gases of different viscosity. *Chem. Eng. Sci.* **1982**, *37*, 1115.
Rowe, P. N.; Foscolo, P. U.; Hoffmann, A. C.; Yates, J. G. X-ray observation of fluidized beds under pressure. *Proceedings of the 4th International Conference on Fluidization*, Kashikojima, Japan; Engineering Foundation: New York, 1983; pp 1-8.
Saxena, S. C.; Vogel, G. J. The measurement of incipient fluidization velocities in a bed of coarse dolomite at elevated temperature and pressure. *Trans. Inst. Chem. Eng.* **1977**, *55*, 184.
Schack, C. J.; Mcneil, M. A.; Rinker, R. G. Methanol synthesis from hydrogen, carbon monoxide and carbon dioxide over a $CuO/ZnO/Al_2O_3$ catalyst, I, steady state kinetic experiments. *Appl. Catal.* **1989**, *50*, 247-263.
Sit, S. P.; Grace, J. R. Interphase mass transfer in aggregative fluidized bed. *Chem. Eng. Sci.* **1978**, *33*, 1115-1122.
Subzwari, M. P.; Clift, R.; Pyle, D. L. Bubbling behaviour of fluidized beds at elevated pressures. *Fluidization*; Davidson, J. F., Kerns, D. L., Eds.; Cambridge University Press, 1978; p 50.
Takagawa, M.; Ohsugi, M. Study on reaction rates of methanol synthesis from carbon monoxide, carbon dioxide and hydrogen. *J. Catal.* **1987**, *107*, 161-172.
Villa, P.; Forzatti, P.; Buzzi-Ferraris, G.; Garone, G.; Pasquon, I. Synthesis of alcohols from carbon oxides and hydrogen, 1, kinetics of the low-pressure methanol synthesis. *Ind. Eng. Chem. Process Des. Dev.* **1985**, *24*, 12-19.
Wagialla, K. M.; Helal, A. M.; Elnashaie, S. S. E. H. The use of mathematical and computer models to explore the applicability of fluidized bed technology for highly exothermic catalytic reactions, I. Oxidative dehydrogenation of butene. *Math. Comput. Modell.* **1991**, *15*, 17-31.
Westerterp, K. R.; Kuczynski, M. A model for a countercurrent gas-solid-solid trickle flow reactor for equilibrium reactions, the methanol synthesis. *Chem. Eng. Sci.* **1987**, *42*, 1871-1885.
Yahia, A. S.; Soliman, M. Personal communication, 1990.
Yang, W.; Chitester, D. C.; Kornosky, R. M.; Keairns, D. L. A generalized methodology for estimating minimum fluidization velocity at elevated pressure and temperature. *AIChE J.* **1985**, *31*, 1086-1092.

Received for review June 5, 1990
Revised manuscript received November 27, 1990
Accepted May 6, 1991

Optimal Long-Term Campaign Planning and Design of Batch Operations

Nilay Shah and Constantinos C. Pantelides*
Centre for Process Systems Engineering, Imperial College of Science, Technology and Medicine, London SW7 2BY, U.K.

Long-term campaign operation of batch plants is appropriate where product demands are stable and plants may be dedicated to a small subset of their potential products for relatively long periods of time. In contrast to previous work which assumed that *all* of the processing steps involved in the manufacture of a product must take place within any campaign producing it, we examine the use of intermediate storage to decouple the manufacture of each product into several stages, each of which can be run independently in campaign mode. Since each stage involves fewer processing steps, more economical plant designs may be produced. We present a systematic and efficient method for optimal campaign planning and design, which considers simultaneously the problems of unit-to-task allocations and task timings. The problem is formulated as a mixed integer linear programming model (MILP) and solved by a modified branch-and-bound technique. A case study is presented to illustrate the applicability of the method.

1. Introduction

There has been a great deal of interest in the computer-aided scheduling and design of batch plants over the past 10 years. This mirrors the resurgence of the batch mode of operation as an efficient means of production, especially where flexibility is required or a large number of low-volume, high-value-added products are to be made in the same facility.

Parakrama's (1985) survey of 99 batch processes oper-

* Author to whom correspondence should be addressed.

0888-5885/91/2630-2308$02.50/0